J. Min. Metall. Sect. B-Metall. 61 (2) (2025) 153 - 165

Journal of Mining and Metallurgy, Section B: Metallurgy

GOLD RECOVERY AND MIGRATION MECHANISM IN THE COPPER SMELTING AND CONVERTING

S.-L. Qu [a], L. Zou [a,*], Z.-Q. Dong [a], L. Li [b]

[a] Shandong Humon Smelting CO., LTD, Yantai, China
[b] Donghua University, College of Environmental Science and Engineering, Shanghai, China

(Received 22 January 2025; Accepted 09 July 2025)

Abstract

The gold embedded in the copper concentrate is enriched in the matte phase during copper smelting and transferred into blister copper during subsequent processing, via which the gold was recycled. In the copper smelting, gold dissolved and appeared as Au (III) in the formed gold-matte solid solution. This solid solution could be formed in two ways: by exchanging Au atoms for Cu atoms in the Cu_5FeS_4 (matte) crystal lattice and by doping Au atoms in Cu_5FeS_4. In the matte converting, the transfer of gold from the matte phase to blister copper occurred spontaneously due to a fact that the surface tension between the gold and matte phases was considerably higher than that between the gold and copper phases. Gold capture by blister copper occurred by Au atoms replacing Cu atoms in the Cu cell.

Keywords: *Gold recycling; Migration behavior; Copper smelting and converting; Structure of gold-matte and gold-copper solid solution*

1. Introduction

Gold has been widely used in electronics, aviation, chemical, medical and other aspects, due to its corrosion resistance, conductivity and catalytic activity, etc. [1-3]. However, gold is a non-renewable resource and has an exceptionally low concentration in the Earth's crust. As the world's largest producer and consumer of gold, China faces a challenge that the gold primary resource is seriously inadequate. The gold reserve in China account for only 4% of global gold reserves, and the associated gold resources account for 41% [4, 5]. In particular, more than half of the gold deposits with the reserves exceeding 50 tons are the associated gold deposits and around 90% of the associated gold deposits come from copper mines [6, 7]. It is important to increase the gold recovery from copper ores to ensure the gold supply in China.

After a mineral processing on the copper ores, a copper concentrate was obtained. Beneficiating method and pyrometallurgy process have been used to enrich and recover gold from the copper concentrate. The beneficiating method mainly referred to cyanide separation. An integrated process of gravity separation, flotation and cyanidation have been used to recycle gold from copper concentrates in previous research, achieving a gold yield of 97.17% at a dosage of 14 kg/t of lime and 2 kg/t of sodium cyanide [8]. However, the high toxicity of cyanides and large quantities of cyanide required caused a significant environmental pollution. Besides, copper concentrates are becoming more and more complicated currently, and gold in it was hard to be recycled efficiently using a mineral separating method. Consequently, a pyrometallurgical process for extracting gold was developed and has been applied in the metallurgical industry, attributed to its significant advantages including large-scale processing, strong adaptability to raw materials and low cost [28, 29]. It is well known that copper can serve as an effective collector for gold. Utilizing this property, gold could be enriched in copper matte during smelting [33], and subsequently transferred from matte to blister copper via converting [14]. After that, gold could be further separated and recycled using a conventional hydrometallurgical refining process. Previous research has reported the migration of gold in copper smelting. Avarma et al. studied the distribution of gold in matte and smelting slag, noting that the distribution of gold in iron olivine slag and copper matte was determined by the property of copper matte, and gold was mainly concentrated in the matte phase [9, 10, 34-36]. Some researchers suggested that, in a molten state, gold and copper

Corresponding author: zoulin0535@163.com

https://doi.org/10.2298/JMMB250122012Q

CC BY SA

phases in matte formed a solid solution [11, 12]. Moreover, Guo et al. found that the distribution of gold was governed by the smelting system and thermodynamic properties, with the distribution of gold in molten matte leading to a reduction in the system's overall Gibbs free energy [13]. In addition, some researchers have studied the distribution of gold between copper and matte at an equilibrium system during the copper converting. The results indicated that copper exhibited a stronger capability on gold compared with matte. However, the microstructure of gold-matte and gold-copper solid solutions formed in copper smelting and converting was not focused a lot [14, 15].

Currently, the density functional theory (DFT) has been proven to be effective study of the behavior of atoms at the atomic level [16-19]. Considering this, it was used to detect the microscopic mechanism of gold enriched by matte in smelting and then captured by blister copper in converting. Moreover, XPS and SEM-EDS analysis were used to study the migration behavior of gold in this pyrometallurgical process.

2. Experimental

2.1. Materials

The copper concentrate used in this study was obtained from a copper smelter located in Shandong province of China. The phase composition of it was shown in **Figure 1(a)**, which showed that $CuFeS_2$, FeS_2 and SiO_2 were the main phases. Its chemical composition was measured by inductively coupled plasma optical emission spectroscopy (ICP-OES, Analytik Jena AG) and elemental analyzer (EA, Vario Max CN), and the results were shown in **Figure 1(b)**. The Cu, Fe and S contents in it were 23.57wt%, 27.64wt% and 20.97wt% respectively, and the Au content was 0.44 g/t. "Others" in **Figure 1(b)** mainly referred to Pb, Sb, Ni and O, etc. Moreover, an additional gold powder (99.99%, MACKLIN) was added into the copper concentrate in the study in order to make the gold migration easier to be measured at all stages. Moreover, SiO_2 with a purity of 99.99% was used as a flux.

2.2. Methods

2.2.1. Experimental methods

In this study, the experimental procedure included two stages of copper smelting followed by copper converting, which were carried out in a vertical resistance furnace as presented in **Figure 2**. 50g copper concentrate was used in the smelting process. For the procedure, the copper concentrate (<75 μm) , SiO_2 (<75 μm), and Au powder (<75 μm) were firstly thoroughly mixed in a glass beaker, placed in a corundum crucible, and then transferred into the furnace. The SiO_2 amount of 9.8 g was fixed at an FeO /SiO_2 mass ratio of 1.8 to accelerate the separation between matte and slag [20]. The Au powder addition amount of 0.4 g was fixed at its content in the copper concentrate of 0.8 wt%. Before heating the furnace to the target temperature, a high-purity Ar at a flow rate of 40 ml/min was used as a protective atmosphere. Considering that the copper smelting and converting generally performs at 1250 °C, the target temperature was set at 1250 °C in this study. Once the target temperature was reached, Ar was changed to a high purity O_2 with a total flow rate of 40 ml/min for the oxidization smelting. After that the oxidization smelting was held for a proper time, the molten sample was cooled down to room temperature in high-purity Ar atmosphere and removed from the furnace. The obtained matte was used for the next converting test.

The procedure for the followed converting was similar to that of the first copper smelting. The amount of SiO_2 added was calculated based on the FeO/SiO_2 mass ratio of 1.8, and the converting temperature was selected as 1250 °C. High-purity O_2

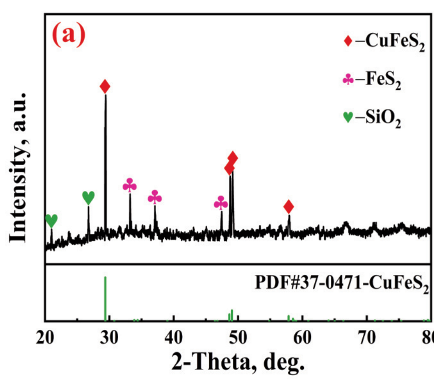

(b)

Component	Content (*wt*%)
Cu	23.57 ± 0.16
Fe	27.64 ± 0.24
S	20.97 ± 0.08
SiO_2	12.01 ± 0.08
CaO	1.34 ± 0.12
Al_2O_3	2.52 ± 0.15
Au	0.44 ppm ± 0.032 ppm
Others	11.95 ± 0.90

Figure 1. *XRD pattern (a) and main chemical compositions (b) of the copper concentrate*

CC BY SA

was used to convert matte to blister copper, and its flow rate was 40 ml/min. After that the converting process was held for a proper time, the molten sample was cooled down to room temperature in high-purity Ar. Then the obtained copper and matte were separated from the corundum crucible and prepared for analysis.

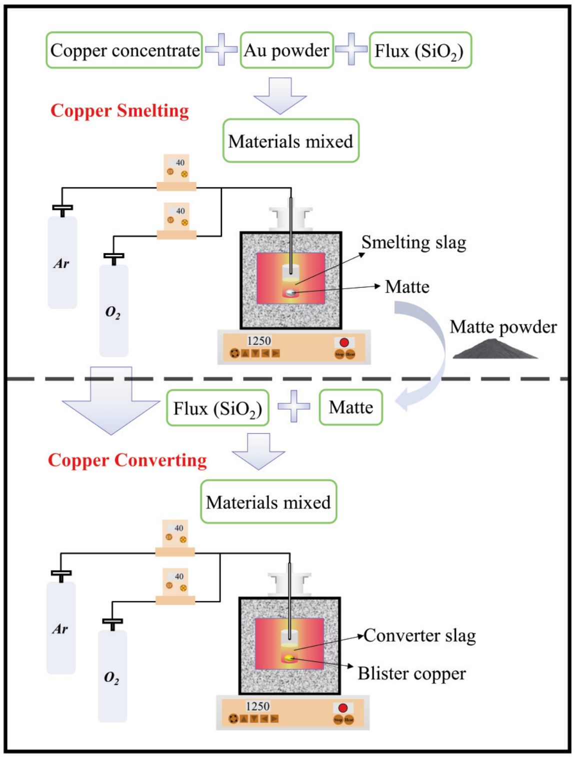

Figure 2. Experiment device

2.3. Characterization

The chemical composition of the sample was examined using inductively coupled plasma optical emission spectrometry (ICP-OES, Analytik Jena AG). The sulfur content in the sample was detected by elemental analyzer (EA, Vario Max CN), and the oxygen content was detected using LECO TC-600 nitrogen/oxygen analyzer. In the detection, the material was firstly grinded to below 75 μm, and three samples were then taken from the grinded material, mixed thoroughly and used to be detected. The analytical step was repeated for three times. All results were reported as the mean and standard deviation from triplicate analyses. The phase composition of the sample was characterized by X-ray diffraction (XRD, Rigaku, TTR -III). The XRD pattern was obtained using Cu-Kα radiation in the 2θ range of 20°-80°. Scanning electron microscopy coupled with energy dispersive X-ray spectroscopy (SEM-EDS) was used to detect the microstructure and phase distributions of the sample. X-ray photoelectron spectroscopy (XPS, ESCALAB 250Xi) was used to analyze the valence states of Cu and Au in the sample.

The Au distribution coefficient in the matte/slag and copper/matte were calculated using Eq. (1) and Eq. (2), respectively [10, 14].

$$L_1 = \frac{Au^a_{matte}}{Au_{slag}} \quad (1)$$

$$L_2 = \frac{Au_{copper}}{Au^b_{matte}} \quad (2)$$

Where, the Au^a_{matte} and Au_{slag} referred to the Au mass concentration in the matte and slag in copper smelting, respectively; the Au_{copper} and Au^b_{matte} referred to the Au mass concentration in the blister copper and matte in copper converting, respectively; L_1 referred to the Au distribution coefficient in the matte and slag in copper smelting; L_2 referred to the Au distribution coefficient in the blister copper and matte in copper converting.

3. Result and discussion

3.1. Au migration in the copper smelting

3.1.1. Determination of the copper smelting ending time

According to previous research [21], the copper smelting process could be judged to achieve a completion by determining the copper content in the obtained matte and smelting slag respectively. Generally, once that the copper content in the matte obtained 65 wt% and the copper content in the smelting slag changed little as the time prolonged, the copper smelting was finished. Copper, iron, and sulfur existed in the forms of FeS_2 and $CuFeS_2$ in the raw copper concentrate, as presented in **Figure 1(a)**. As the smelting was performed, these minerals would be oxidized and then converted to matte and slag phases respectively, via Eq. (3)-(7). It caused the copper content in the matte increased and that of iron and sulfur decreased with the extending of smelting time, as indicated by **Figure 3(a)**. Accordingly, the iron content in the slag increased accompanied by a small change of the copper content in the slag (**Fig. 3(b)**). With the smelting time from 0 s to 600 s, **Figure 3(a)** presented that the copper content in the matte increased from 23.57 to 65.27 wt%, the iron content decreased from 27.64 to 12.97wt%, and the sulfur content decreased from 20.97 to 18.25 wt%. **Figure 3(b)** presented that the iron content in the smelting slag increased to 42.25 wt% as the smelting time increased from 0 s to 600 s, and then its content and the copper content in the slag increased little as the

CC BY SA

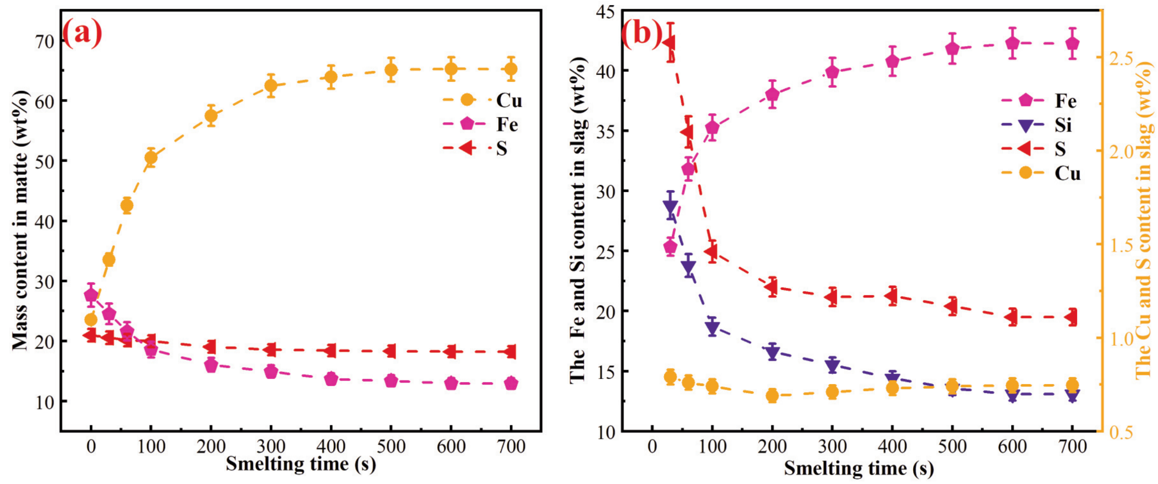

Figure 3. *(a) Cu, Fe and S concentration in matte as a function of time; (b) Logarithmic distribution coefficients of Au*

smelting time prolonged further. The smelting ending time was found to be 600 s.

$$4CuFeS_2 + 5O_2 = 2Cu_2S + FeS + 2FeO + 4SO_2 \quad (3)$$

$$2Cu_2S + 3O_2 = 2Cu_2O + 2SO_2 \quad (4)$$

$$2FeS + 3O_2 = 2FeO + 2SO_2 \quad (5)$$

$$FeS + Cu_2O = FeO + Cu_2S \quad (6)$$

$$2FeO + SiO_2 = 2FeO \cdot SiO_2 \quad (7)$$

3.1.2. Au distribution in the matte and smelting slag

As described above, the copper smelting was completed at the smelting time of 600 s. In this time range, the changes of Au distribution in the matte and smelting slag with the smelting time was presented in **Figure 4 (a)**. It showed that the L_1 increased with the time extension and remained almost constant after 600 s, indicating that Au continuously migrated from the smelting slag to the matte phase in the copper smelting. The SEM-EDS results in **Figure 5** presented that Au was distributed randomly in the matte. Moreover, some segregated metal particles could also be detected, shown as white spot “1” in **Figure 5**. The primary elements in the white spot included Au, Cu, Sb and Pb, indicating that some matte had been over oxidized to metallic Cu in the copper smelting. Additionally, the result from the surface scanning also presented that Au was also commonly presented in the matte phase (spot “2”). So, Au existed in two forms in the matte: one as part of an alloy (spot “1”) and the other as a substitution for other metals (copper or iron) in the matte structure (spot “2”). To further validate it, X-ray photoelectron spectroscopy (XPS) was used to analyze the obtained matte. The XPS

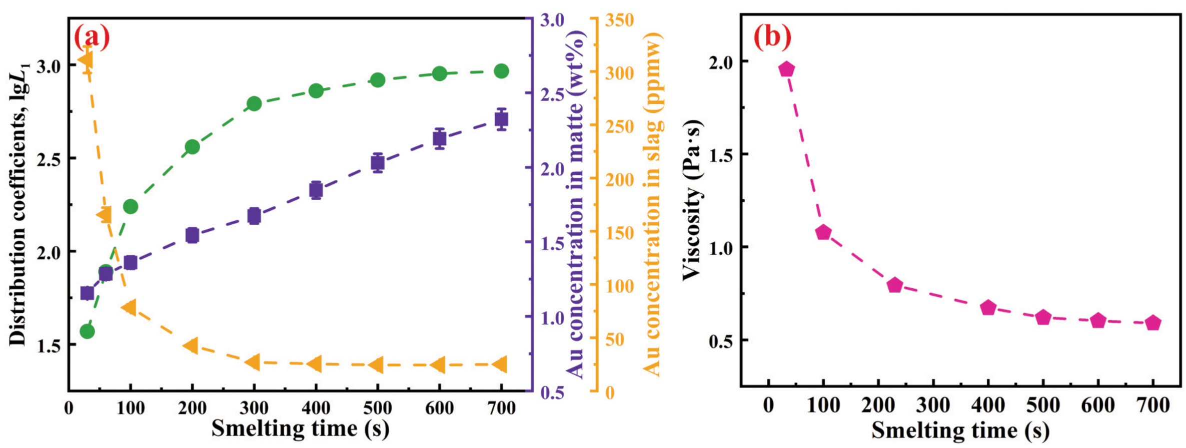

Figure 4. *(a) Logarithmic distribution coefficients of Au in matte and smelting slag; (b) Changes of smelting slag viscosity with time*

CC BY SA

spectra of Cu 2p and Au 4f was presented in **Figures 6(a)** and **6(b)** respectively. In **Figure 6(a)**, the binding energy corresponding to Cu 2p was detected at 932.35 eV and 933.28 eV respectively. These signals were attributed to the energy signals for Cu (I) and Cu (0) respectively [22, 23]. It indicated that a small amount of Cu has been generated in this smelting process. In **Figure 6(b)**, signals representing Au were characterized at 88.76 eV and 91.64 eV, respectively. The former corresponded to the Au (0) signal, while the latter represented the Au (III) signal. The XPS analysis results above revealed that Au in this matte phase existed in two forms of alloy (Au (0)) and compound (Au (III)), which was consistent with the SEM-EDS results in **Figure 5**. Moreover, the Au (0) alloy accounted for 25.17% of the total gold, while the Au (III) compound accounted for 74.83% as presented in **Figure 6(b)**.

Figure 6(c) presented that the matte was mainly composed of Cu_5FeS_4, $Cu_{1.96}S$, Cu_4S_7 and FeS, and Cu_5FeS_4 was the main phase. Due to it, Cu_5FeS_4 was used in the followed first-principles calculation (DFT) to characterize the microstructure of the Au-containing matte. Based on the studies by Huang et al. and Liu et al. [11-12], Au (III) embedded in the matte was mainly via it dissolving in the matte phase to form a solid solution. Generally, this solid solution could be formed via two pathways, including substituting a Cu atom in Cu_5FeS_4 with an Au atom (**Fig. 7(a)**) and doping an Au atom into the Cu_5FeS_4 crystal lattice (**Fig. 7(b)**). To study the formation mechanism, the first-principles calculation was used to calculate the binding energy (E_{coh}) between Au and Cu_5FeS_4. The binding energy could reflect the

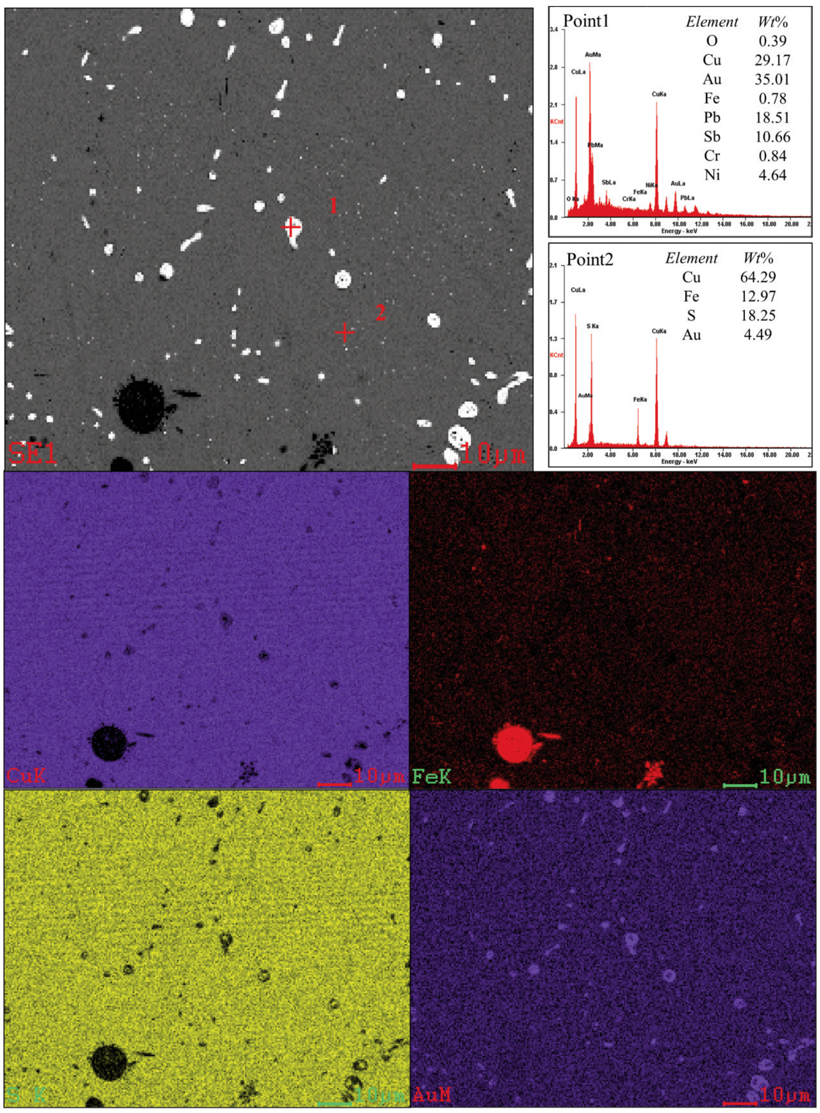

Figure 5. *SEM-EDS results of the matte obtained at the smelting time of 600 s*

CC BY SA

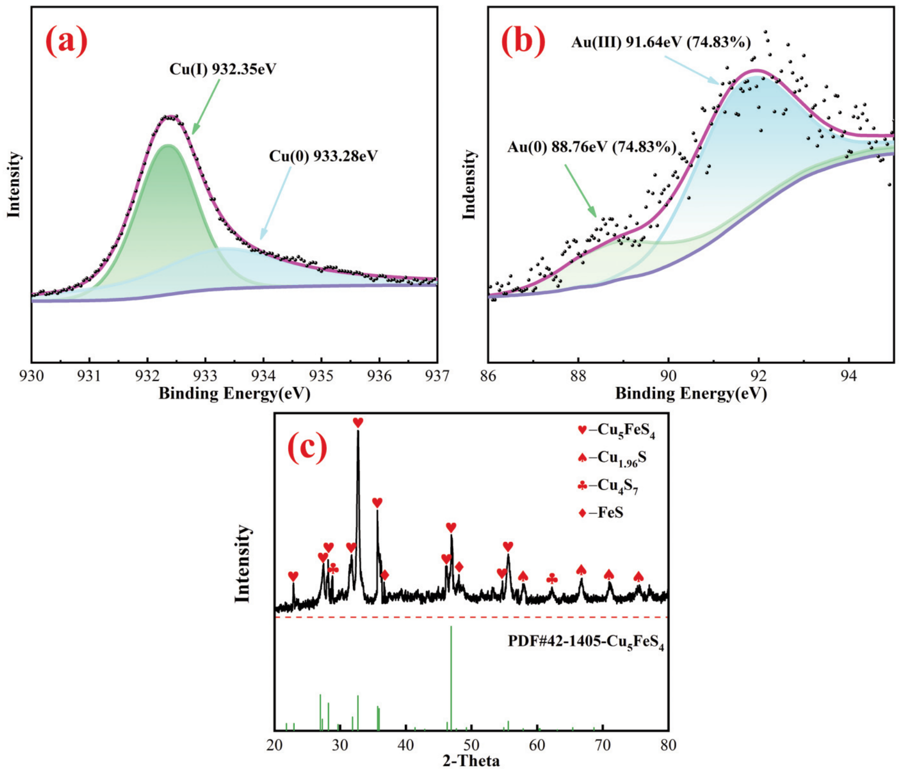

Figure 6. *High-resolution XPS spectra of (a) Cu 2p and (b)Au 4f in the matte; (c) XRD pattern of the obtained matte*

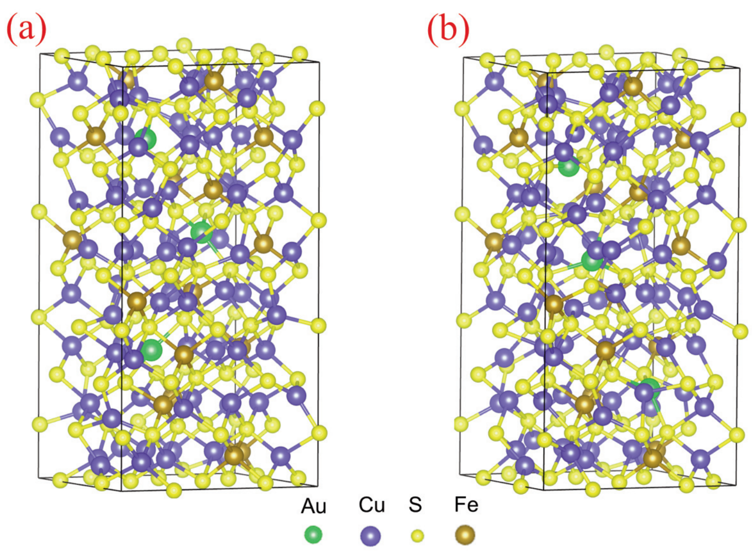

Figure 7. *Schematic diagram of the first-principles computational structure: a, Au replaced to Cu_5FeS_4; b, Au doped to Cu_5FeS_4*

stability of the bond between gold atoms and Cu_5FeS_4 matrix, and it could be calculated using Eq. (8) [28, 29].

$$E_{coh} = \frac{E_{tot} - xE_{Au} - yE_{CuFeS_4}}{x + y} \quad (8)$$

Where, E_{coh} is the binding energy, E_{tot} represents the total energy of the solid solution system, E_{Au} and $E_{Cu5FeS4}$ refer to the energies of the isolated gold atom and the initial Cu_5FeS_4 matrix respectively, and *x* and *y* are the number of Cu_5FeS_4 and Au atoms in the Cu_5FeS_4 cell structure model respectively. When the E_{coh} is negative, the solid solution system possesses a lower energy than the isolated components,

CC BY SA

suggesting that the incorporation of gold atoms enhances the system's stability; conversely, a positive Ecoh value implies an unstable bonded state where gold atoms tend to dissociate from the matrix. The calculation results were presented in Table 1. E_{coh} was calculated to be -1.5136 for the Au replaced to Cu, while it was -1.4835 for the Au doping. Hence, the entry of Au into the matte phase proceeded spontaneously. Besides, both solid solution structures could be formed in the process of gold entering into the matte.

Table 1. *The formation energy of Cu_5FeS_4-Au*

Structures	Methods	Formation Energy/eV
Au replaced to Cu_5FeS_4	Substitution	-1.5136
Au doped to Cu_5FeS_4	Interstitial	-1.4835

After the process of gold entering into the matte, the matte droplets settled down from the molten slag because of the density difference between them. The settling velocity of the matte droplets was related to the factors such as the droplet size, density difference and smelting slag viscosity, and the relation among them could be expressed using the Stokes' formula [24, 30]. The Stokes' formula is based on the force balance between the buoyancy and gravity, as follows:

$$v = \frac{2gr^2}{9\eta}\left(\rho_m - \rho_s\right) \tag{9}$$

In Eq. (9), v is the settling velocity of the matte droplets, g is the acceleration due to gravity, r is the radius of the droplets, η is the viscosity of the molten slag, and ρ_m and ρ_s are the densities of the matte and the slag, respectively. Eq. (9) represents a simplified expression of Stokes' law, which describes the motion behavior of particles in a viscous fluid. According to Stokes' law, the drag force (F) experienced in a particle moving through a fluid could be expressed as $F = 6\pi\eta vr$. When particles undergo sedimentation in a molten slag medium, their mechanical state is determined by three interacting forces: gravitational force ($4\pi r^3\rho_m g/3$), buoyant force ($4\pi r^3\rho_s g/3$) and viscous drag force ($6\pi\eta\upsilon r$). Upon reaching terminal settling velocity, the system attains a state of mechanical equilibrium where the gravitational force equals the sum of buoyant and drag forces ($4\pi r^3\rho_m g/3 = 6\pi\eta\upsilon r + 4\pi r^3\rho_s g/3$). Based on this force balance condition, Eq. (9) could be derived.

During the smelting process, FeS from the copper concentrate would be oxidized to FeO. Then FeO reacted with the flux of SiO_2 to produce ferro silicates, which entered the slag and reduced the slag viscosity. Moreover, the density of matte increased with it, and the density difference between matte and slag phases enlarged. Based on Stokes' formula in Eq. (9), the settling velocity of the matte particles was increased during the smelting process, accompanied with which Au was separated from molten slag and concentrated in the matte phase.

3.2. Au migration in the copper converting

3.2.1. Determination of the matte converting ending time

Under the condition of converting temperature of 1250 °C, SiO_2 addition amount of 9% and O_2 flow rate of 40 ml/min, the converting of matte obtained from the copper smelting was studied. The SiO_2 amount was selected as 9% to control the FeO/SiO_2 mass ratio being equal to 1.8 after the iron in matte completely being oxidized and entering into molten slag.The matte converting could be judged to achieve completion by determining the sulfur and oxygen contents in the obtained blister copper. Generally, once that the sulfur and oxygen contents in the obtained blister copper changed little with the time and the copper distribution percentage in the blister copper achieved a maximum, the matte converting was finished [25]. As the converting time increased from 60 s to 600 s, **Figure 8(a)** showed that the sulfur content in the blister copper decreased from 1.09 wt% to 0.52 wt%, and the oxygen content in the blister copper had a little increase and achieved 1.18 wt% at the time of 600 s. The sulfur and oxygen in the blister copper were mainly derived from the dissolved Cu_2S and Cu_2O in it. As the converting time increased, the dissolved Cu_2S would be oxidized to Cu_2O using Eq. (4) and then converted to Cu using Eq.(10). It caused the sulfur content in the blister copper decreased in **Figure 8(a)**. While, as the converting time increased further, Cu would be oxidized to Cu_2O and some of it dissolved in the blister copper, leading to an increase of the oxygen content in **Figure 8(a)**. Besides, in this converting time rangment, **Figure 8(b)** showed that the copper distribution in the blister copper and the copper content in the blister copper increased. The copper distribution in the blister copper was calculated using the mass ratio of Cu in the blister copper to Cu in the matte. However, as the time exceeded 600 s, the oxygen content in the blister copper inceased further (**Fig. 8(a)**) and the copper distribution in the blister copper had an obvious decrease in **Figure 8(b)**. The matte converting ending time was found to be 600 s.

$$Cu_2S + 2Cu_2O = 6Cu + SO_2 \tag{10}$$

3.2.2. Au distribution in the matte and blister copper

In the converting process, FeS from the matte would be oxidized to FeO and then reacted with SiO_2 to form ferro silicates, which entered the slag and decreased the slag viscosity as presented in **Figure 8 (c)**. This increased the separation of blister copper from molten slag. Moreover, according to previous research [14], Au simultaneously transferred from matte to blister copper in the copper converting. The changes of Au distribution between blister copper and matte with time in **Figure 8(d)** were similar to the Cu distribution in blister copper in **Figure 8(b)** before 600 s.

Figure 9 presented the SEM-EDS results of the matte which was obtained with the converting time of 120 s, in which four typical points were identified. The phase locating at points "1" and "2" was matte deduced from the element composition of it, and the phase at points "3" and "4" was Cu. It is noteworthy that the Au content at the point "4" was obviously higher than that at the point "3", and the light-colored area holding point "4" was surrounded by the light-gray area containing point "3". The Au distribution in **Figure 9** indicated that Au would be transferred from matte phase to the blister copper in the copper converting. In other words, Cu has a stronger capture effect on Au during the matte converting.

Moreover, the produced blister copper at the converting time of 600 s was polished and then analyzed using XPS to investigate the valence states of Cu and Au in it. The results were presented in **Figure 10**. In **Figure 10(a)**, binding energy corresponding to Cu 2p was detected at 932.2 eV, was a signal for Cu(0) [26]. Furthermore, in **Figure 10(b)** for the XPS spectra of Au, two signals were observed at 83.60 eV and 84.68 eV, respectively. These signals shifted slightly from the standard signals of Au(0) at 84.00 eV [27], which could be attributed to the influence of Cu on Au as Au entered into the Cu phase.

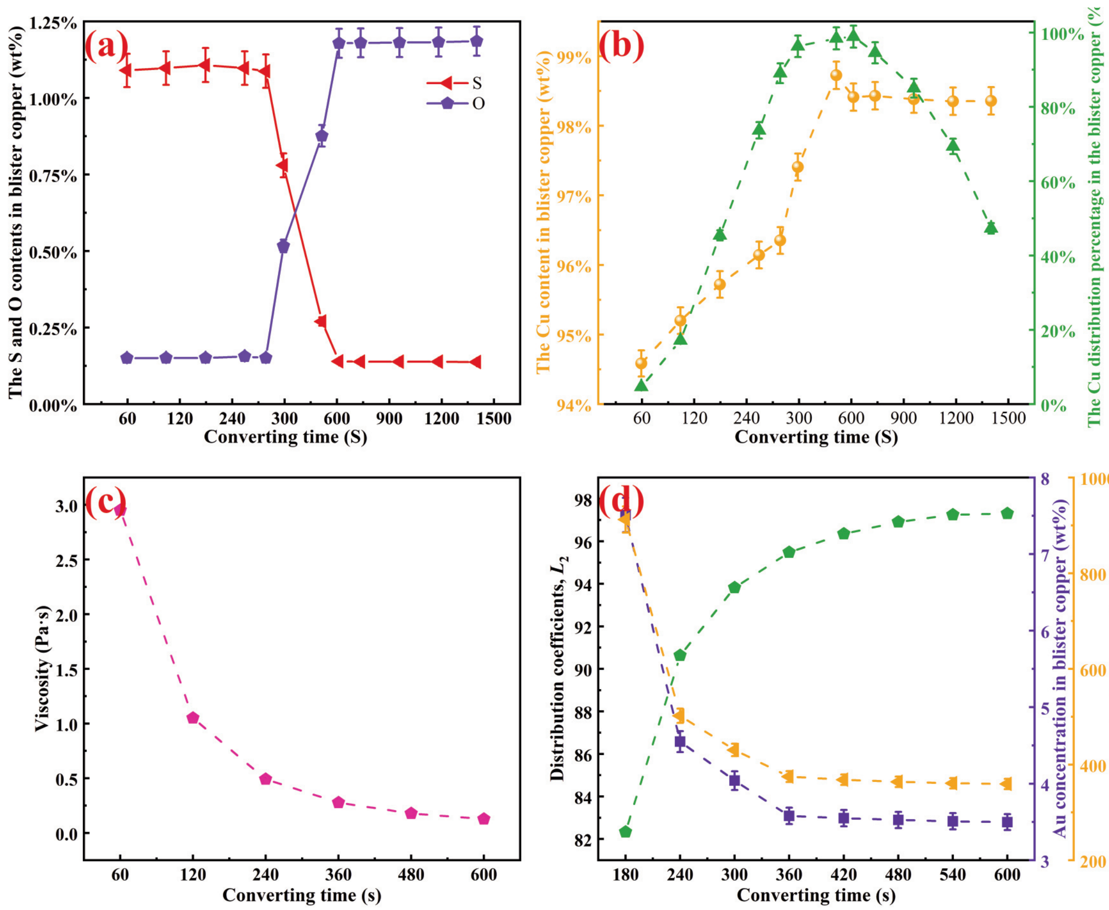

__Figure 8.__ (a) Effects of converting time on the sulfur and oxygen contents in the blister copper; (b) Effects of smelting time on the copper content in the blister copper and the copper distribution percentage in the blister copper; (c) Changes of converting slag viscosity with time; (d) Effects of converting time on the gold distribution between copper and matte

CC BY SA

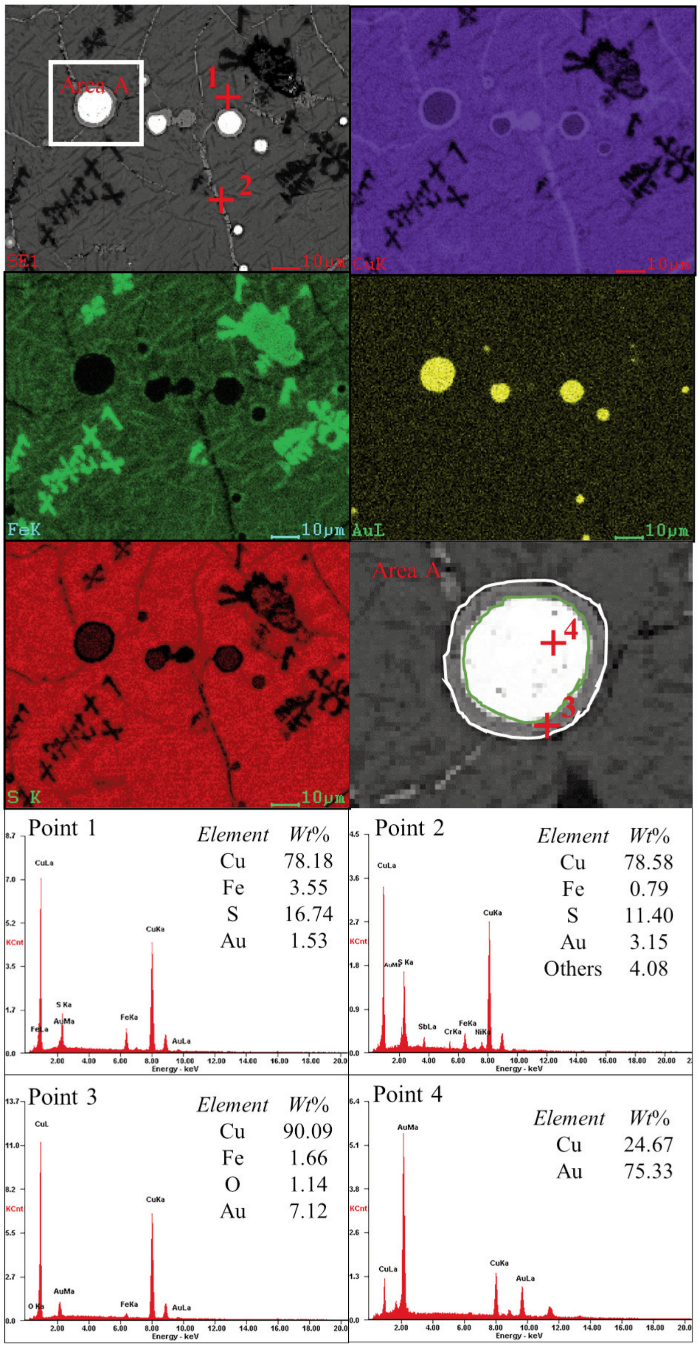

Figure 9. SEM-EDS results of the matte obtained at the converting time of 120 s

3.2.3. Mechanism of capture process of copper for Au

As described above, Cu has a capture effect on Au during the matte converting. To clarify it, surface thermodynamics and first principles were used to investigate the mechanism. Based on previous research [28-30], the capture process could be divided into two steps, as shown in **Figure 11**: the [Au] transfer through the matte phase into the [Cu] phase for the first step and the alloying of [Cu] and [Au] for the second step.

For the first step, the Gibbs free energy change (ΔG) corresponding to the ternary system of matte–[Cu]–[Au], was presented in Eq. (11). In Eq. (11), ΔG^{Au}_{matte} and ΔG^{Au}_{Cu} are the Gibbs free energy changes of [Au] migrated out from the matte and into the [Cu] phase, respectively; μ^{Au}_{matte} and μ^{Au}_{Cu} are the

cc BY SA

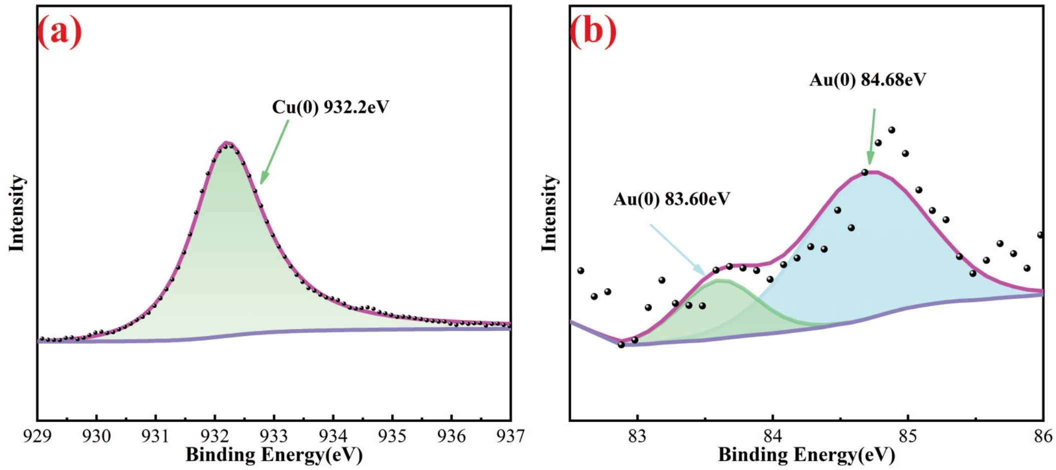

Figure 10. *(a) Cu 2p and (b)Au 4f high-resolution XPS spectra in blister copper*

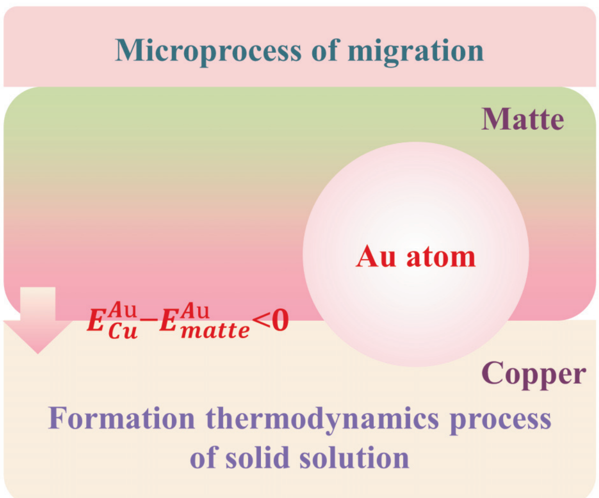

Figure 11. *Thermodynamic mechanism of the capture process of blister copper for Au*

chemical potentials of [Au] in the matte and [Cu] respectively, which are equal to the surface energy of [Au] (E^{Au}_{matte} and E^{Au}_{Cu}) caused by the surface tension of [Au] interacting with the molten matte and [Cu], respectively; dn^{Au}_{matte} and dn^{Au}_{Cu} are the molar variations of [Au] transferred out from the matte and into the [Cu], respectively. Owing to the $dn^{Au}_{matte}=-dn^{Au}_{Cu}$, the Eq. (11) could be converted to Eq. (12). The surface tension between the metal and matte phases was considerably higher than that between the metallic phases [22-24], causing $E^{Au}_{Cu} < E^{Au}_{matte}$ and $\Delta G < 0$. This indicated that the transfer of [Au] from the matte into the [Cu] proceeded spontaneously.

$$\Delta G = \Delta G^{Au}_{matte} + \Delta G^{Au}_{Cu} = \mu^{Au}_{matte} dn^{Au}_{matte} + \mu^{Au}_{Cu} dn^{Au}_{Cu} \quad (11)$$

$$\Delta G = \left(\mu^{Au}_{Cu} - \mu^{Au}_{matte}\right) dn^{Au}_{Cu} = \left(E^{Au}_{Cu} - E^{Au}_{matte}\right) dn^{Au}_{Cu} \quad (12)$$

In the second step, the first principles were used to calculate the alloying mechanism between [Au] and [Cu]. Within the generalized gradient approximation using the Perdew–Burke–Ernzerhof formulation [31], the spin-polarization density functional theory calculations were performed using the Vienna Ab Initio Package. Two ways to form Cu–Au alloy was considered, including the replacement of a Cu atom with an Au atom in the Cu cell (**Fig. 12(a)**) and the doping of Au atom in the center of the Cu cell (**Fig. 12(b)**). The binding energy (E_{coh}) was calculated using Eq. (13). Here, E_{tot} is the total energy of the alloy; E^{Cu}_{atom} and E^{Au}_{atom} represent the energies of Cu and Au atoms, respectively; and *x* and *y* are the number of Cu and Au atoms in the Cu cell structure model, respectively. The results in **Table 2** presented that E_{coh} in the structure model of Au replaced into the Cu cell was negative, indicating the formation of Cu–Au alloy was realized through the Au atom replaced Cu

CC BY SA

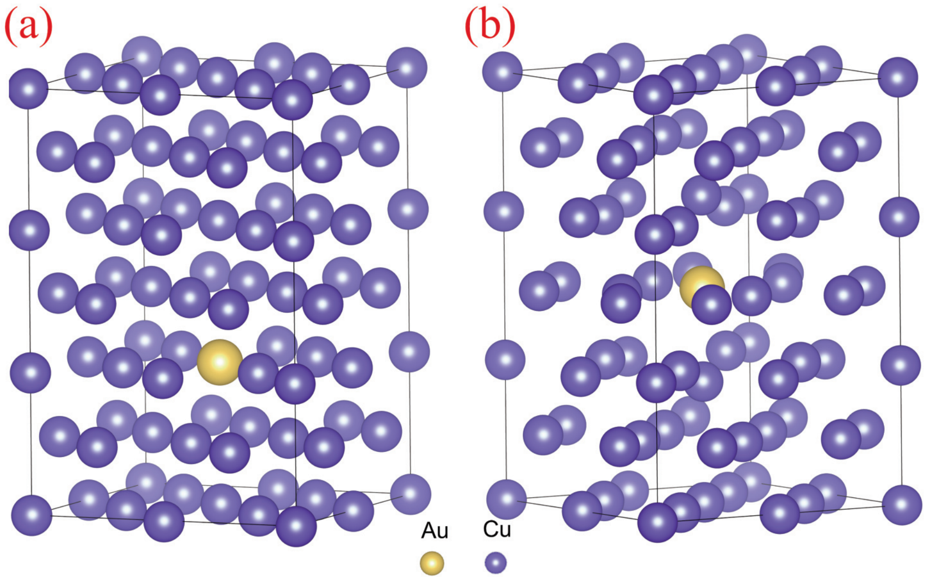

Figure 12. *Schematic diagram of the first-principles computational structure, (a), Au replaced to Cu; b, Au doped to Cu*

atom in the Cu cell, and a stable structure could be formed. In other words, the Au capture by blister copper was realized by Au atoms replaced Cu atoms in the Cu cell.

$$E_{coh} = \frac{E_{tot} - xE_{atom}^{Cu} - yE_{atom}^{Au}}{x+y} \quad (13)$$

Table 2. *The formation energy of Cu-Au*

Structures	Methods	Formation Energy/eV
Au replaced to Cu	Substitution	-0.3913
Au doped to Cu	Interstitial	3.7794

4. Conclusion

The associated gold from copper concentrates occupied a high proportion of the gold production. To increase gold recovery from it, the gold migration behavior in the smelting and converting of copper concentrates was investigated in this research. In the copper smelting, Au was mainly concentrated and occurred as Au (III) in the obtained Au-containing matte phase. Au dissolved in the matte phase and formed a solid solution. Based on the first-principles calculation, the binding energy was -1.5136 eV for an Au atom replaced to a Cu atom in the Cu_5FeS_4 (matte) crystal lattice, and it was -1.4835 for the Au doping into the Cu_5FeS_4 crystal lattice. The entry of Au into the matte phase proceeded spontaneously, and both solid solution structures could be formed between Au and matte in the copper smelting. In the matte converting, the transfer of [Au] from the matte into the blister copper proceeded spontaneously deduced from the changes of Gibbs free energy, and the Au capture by blister copper was realized by Au atom replaced Cu atom in the Cu cell. Therefore, in the copper smelting and converting, the loss of matte into smelting slag and the loss of blister copper into converting slag should be limited, to decrease the gold loss.

Author contribution

Shengli QU: Data curation, Investigation, Validation, Writing – original draft. Lin ZOU: Supervision, Writing – review & editing. Zhunqin DONG: Data curation, Investigation, Validation. Lei LI: Writing – review & editing

Declaration of Competing Interest

The authors declare that they have no known competing financial interests or personal relationships that could have appeared to influence the work reported in this paper.

Data availability

Data availability will be provided on request.

Acknowledgments

The authors wish to express thanks to Shandong Humon Smelting CO., LTD, for the financial support of this research.

cc BY SA

References

[1] J.W. Liu, Q.L. Ma, Z.Q. Huang, G.G. Liu, H. Zhang, Recent progress in graphene-based noble-metal nanocomposites for electrocatalytic applications, Advanced Materials, 31 (9) (2019) 1800696. https://doi.org/10.1002/adma. 201800696

[2] K. Mao, Z.G. Yang, H. Zhang, X.Q. Li, J.M. Cooper, Paper-based nanosensors to evaluate community-wide illicit drug use for wastewater-based epidemiology, Water Research, 189 (2021) 116559. https://doi.org/10.1016/j.watres.2020.116559

[3] N. Daems, C. Michiels, S. Lucas, S. Baatout, A. Aerts, Gold nanoparticles meet medical radionuclides, Nuclear Medicine and Biology, 100-101 (2021) 61-91. https://doi.org/10.1016/j.nucmedbio.2021.06.001

[4] Y.T. Zhang, Development status and future prospect of China's gold industry, Gold, 32 (06) (2011) 1-4.

[5] B.M. Zhou, F.L. An, Current situations of worldwide gold production and considerations on gold industry development in China, Gold, 33 (03) (2012) 1-6.

[6] W.Z. Xing, Relation of property of associated gold and silver ore with recovery of mineral processing, Journal of Bgrimm, 3 (1) (1994) 25-33.

[7] S.Z. Feng, The types and main ore control factors of associated gold deposits in the east of China, Gold Geology, 9 (3) (2003) 9-14.

[8] J.K. Wen, R.M. Ruan, Study on the technology of increasing gold and copper recovery from pyrrhotite type of copper-gold ores, Gold, 18 (8) (1997) 30 -34.

[9] K. Avarmaa, H. Johto, P. Taskinen, Distribution of precious metals (Ag, Au, Pd, Pt, and Rh) between copper matte and iron silicate slag, Metallurgical and Materials Transactions B, 47 (2016) 244-255. https://doi.org/10.1007/s11663-015-0498-4

[10] K. Avarmaa, H. O'Brien, H. Johto, P. Taskinen, Equilibrium distribution of precious metals between slag and copper matte at 1250–1350 °C, Journal of Sustainable Metallurgy, 1 (2015) 216-228. https://doi.org/10.1007/s40831-015-0020-x

[11] H. Huang, H.H. Xiong, L. Gan, Effect of vacancy, As, and Sb dopants on the gold-capturing ability of Cu2S during gold collection in matte processes, Molecules, 28 (21) (2023) 7390. https://doi.org/10.3390/molecules28217390

[12] S.J. Liu, The metallurgy of platinum group metals, Metallurgical Industry Press, Beijing, 2001, p.167.

[13] X.Y. Guo, S.S. Wang, Q.M. Wang, Q.H. Tian, Z. Wang, Y.J. Wang, G.M. Peng, B.J. Zhao, Mechanism of gold collection in matte and distribution behavior of precious metals in oxygen-enriched smelting process, The Chinese Journal of Nonferrous Metals, 30 (12) (2020) 2951-2962.

[14] D. Shishin, T. Hidayat, J. Chen, P.C. Hayes, E. Jak, Experimental investigation and thermodynamic modeling of the distributions of Ag and Au between slag, matte, and metal in the Cu–Fe–O–S–Si system, Journal of Sustainable Metallurgy, 5 (2019) 240-249. https://doi.org/10.1007/s40831-019-00218-w

[15] G.R. Ye, J.Q. He, X.S. Liu, Behavior of gold and silver in copper making stage in a converter, Nonferrous Metals, 41 (2) (1989)

[16] B. Niu, Z.M. Xu, In situ preparation of a Nb–Pb codoped and Pd loaded TiO_2 photocatalyst from waste multi-layer ceramic capacitors by a chlorination–leaching process, Green Chemistry, (4) (2019) 874-884. https://doi.org/10.1039/c8gc02263a

[17] Z.B. Dai, Y.Z. Feng, H.H. Xiong, L. Gan, Atomic-level into the microscopic mechanism of gold capture by FeS during gold collection in matte process, Materials Today Communications, 40 (2024) 109761. https://doi.org/10.1016/j.mtcomm .2024.109761

[18] H.L. Li, S.H. Feng, Z.Q. Yang, J.P. Yang, S.J. Liu, Y.C. Hu, L. Zhong, W.Q. Qu, Density functional theory study of mercury adsorption on CuS surface: effect of typical flue gas components, Energy & Fuels, 33 (2) (2019) 1540–1546.

https://doi.org/ 10.1021/acs.energyfuels.8b03585

[19] H.P. Peng, X.H. Zhao, Y.G. Zhao, Y. Lei, C.J. Wu, Y. Liu, J.X. Chen, Z.W. Li, X.P. Su, New insights into the adsorption of Fe on Ti(CxN1−x) surface: first-principles study, Materials Today Communications, 35 (2023) 106364.

https://doi.org/ 10.1016/j.mtcomm.2023.106364

[20] K. Wang, Y. Liu, J. Hao, Z.H. Dou, G.Z. Lv, T.A. Zhang, A novel slag cleaning method to recover copper from molten copper converter slag, Transactions of Nonferrous Metals Society of China, 33 (8) (2023) 2511-2522.

https://doi.org/10.1016/s1003-6326(23)66277-6

[21] F.J. Tavera, E. Bedolla, Distribution of Cu, S, O and minor elements between silica-saturated slag, matte and copper-experimental measurements, International Journal of Mineral Processing, 29 (3-4) (1990) 289-309. https://doi.org/10.1016/0301-7516(90)90060-C

[22] I. Nakai, Y. Sugitani, K. Nagashima, Y. Niwa, X-ray photoelectron spectroscopic study of copper minerals, Journal of Inorganic and Nuclear Chemistry, 40 (5) (1978) 789-791.

https://doi.org/10.1016/0022-1902(78)80152-3

[23] X.M. Liu, J.X. Wu, J.S. Zhu, Photoemission study on formation of Y-Cu intermetallic compound on Cu(1 0 0) surface, Physica B: Condensed Matter, 226 (4) (1996) 399-405.

https://doi.org/10.1016/0921-4526(96)00465-6

[24] S.W. Zhou, Y.G. Wei, Y. Shi, B. Li, H. Wang, Characterization and recovery of copper from converter copper slag via smelting separation, Metallurgical and Materials Transactions B, 49 (5) (2018) 2458-2468.

https://doi.org/10.1007/s11663-018-1364-y

[25] W.K. Qu, Y.B. Yang, S.W. Zhou, Y.G. Wei, B. Li, Phase transformation of arsenic, antimony and lead in high-grade copper matte converting, Minerals, 14 (5) (2024) 499. https://doi.org/10.3390/min14050499

[26] M.J. Peng, Y.F. Sun, W. Zang, C.Y. Gao, L.J. Miao, A.G. Wu, Y.J. Zhang, A highly sensitive method for the detection of p-Aminophenol based on Cu–Au nanoparticles and KIO_3, Analytica Chimica Acta, 1283 (2023) 341954.

https://doi.org/ 10.1016/j.aca.2023.341954

[27] S. Almeriri, A.A.L. Ahmad, B.L. Droumaguet, R. Pires, A.A. Mohamed, M.M. Chehimi, Developed of latent fingerprints via aryldiazonium tetrachloroaurate salts on copper surfaces: An XPS study, Langmuir, 36 (1) (2019) 74-83.

https://doi.org/10.1021/ acs.langmuir.9b03390

[28] L.G. Zhang, Q.M. Song, Y. Liu, Z.M. Xu, An integrated capture of copper scrap and electrodeposition process

to enrich and prepare pure palladium for recycling of spent catalyst from automobile, Waste Management, 108 (2020) 172-182. https://doi.org/10.1016/j.wasman.2020.04.013

[29] L.G. Zhang, Q.M. Song, Y. Liu, Z.M. Xu, Novel approach for recovery of palladium in spent catalyst from automobile by a capture technology of eutectic copper, Journal of Cleaner Production, 239 (2019) 118093. https://doi.org/10.1016/j.jcl epro.2019.118093

[30] Y. Liu, Q.M. Song, L.G. Zhang, Z.M. Xu, Behavior of enrichment and migration path of Cu–Ag–Pd–Bi–Pb in the recovery of waste multilayer ceramic capacitors by eutectic capture of copper, Journal of Cleaner Production, 287 (2021) 125469. https://doi.org/10.1016/j.jclepro.2020.125469

[31] J.P. Perdew, K. Burke, M. Ernzerhof, Generalized gradient approximation made simple, Physical Review Letters, 78 (1997) 1396. https://doi.org/10.1103/PhysRevLett.77.3865

[32] S.S. Wang, Q.M. Wang, X.Y. Guo, K.Q. Tan, Operation and fundamentals of Direct anode copper production from matte, Metallurgical and Materials Transactions B, 54 (2023) 487-498. https://doi.org/10.1007/s11663-023-02721-8

[33] A.M. Amdur, S.A. Fedorov, V.V. Yurak, Transfer of gold, platinum and non-ferrous metals from matte to slag by flotation, Metals, 10 (11) (2021), 1-14. https://doi.org/10.3390/met11101602

[34] P. Piskunen, K. Avarmaa, H. O'Brien, L. Klemettinen, H. Johto, P. Taskinen, Precious metal distributions in direct nickel matte smelting with low-Cu mattes, Metallurgical and Materials Transactions B, 49 (2018) 98-112.

https://doi.org/10.1007/s11663-017-1115-5

[35] M. Chen, K. Avarmaa, L. Klemettinen, H. O'Brien, J. Shi, P. Taskinen, D. Lindberg, A. Jokilaakso, Precious metal distributions between copper matte and slag at high Pso_2 in WEEE reprocessing, Metallurgical and Materials Transactions B, 52 (2) (2021), 871-882. https://doi.org/10.1007/s11663-021-02059-z

[36] L.S. Tsemekhman, L.B. Tsymbulov, R.A. Pakhomov, V.A. Popov, Behavior of platinum metals during sulfide copper-nickel raw materials processing, Tsvetnye Metally, (11) (2016) 50-56. https://doi.org/10.17580/tsm.2016.11.05

IZDVAJANJE ZLATA I MEHANIZAM MIGRACIJE TOKOM PROCESA TOPLJENJA I KONVERTOVANJA BAKRA

S.-L. Qu [a], L. Zou [a,*], Z.-Q. Dong [a], L. Li [b]

[a] Shandong Humon Smelting CO., LTD, Jantaj, Kina
[b] Donghua Univerzitet, Fakultet za nauku o životnoj sredini i inženjerstvo, Šangaj, Kina

Apstrakt

Zlato prisutno u koncentratu bakra obogaćuje se u bakrencu tokom procesa topljenja koncentrata bakra, a zatim prelazi u tzv. blister-bakar u toku narednih faza prerade, čime se zlato efektivno reciklira. Tokom topljenja koncentrata bakra, zlato se rastvara i prisutno je u obliku Au (III) u čvrstom rastvoru zlato-bakrenac. Ova čvrsta rastvorna faza može nastati na dva načina: zamenom atoma bakra atomima zlata u kristalnoj rešetki Cu_5FeS_4 (bakrenac) i dopiranjem atoma zlata u Cu_5FeS_4. Tokom konvertovanja bakrenca, prelazak zlata iz bakrenca u blister-bakar odvija se spontano, usled činjenice da je površinski napon između zlata i bakrenca znatno viši nego između zlata i bakra. Hvatanje zlata od strane blister-bakra ostvaruje se zamenom Cu atoma sa Au atomima u kristalnoj rešetki bakra.

Ključne reči: *Reciklaža zlata; Mehanizam migracije; Topljenje i konvertovanje bakra; Struktura zlato-bakrenac i zlato-bakar čvrstih rastvora*

CC BY SA